Data assimilation in 2D viscous Burgers equation using a stabilized explicit finite difference scheme run backward in time

Alfred S. Carasso*

November 13, 2021

Abstract

The 2D viscous Burgers equation is a system of two nonlinear equations in two unknowns, $u(x,y,t),\ v(x,y,t)$. This paper considers the data assimilation problem of finding initial values $[u(.,0),\ v(.,0)]$, that can evolve into a close approximation to a desired target result $[u^*(.,T),\ v^*(.,T)]$, at some realistic $T > 0$. Highly non smooth target data are considered, that *may not correspond to actual solutions at time* T. Such an ill-posed 2D viscous Burgers problem has not previously been studied. An effective approach is discussed and demonstrated, based on recently developed stabilized explicit finite difference schemes that can be run backward in time. Successful data assimilation experiments are presented involving 8 bit, 256×256 pixel gray-scale images, defined by non-differentiable intensity data. An instructive example of failure is also included.

1 Introduction

The 2D viscous Burgers equation [1], is a coupled system of two nonlinear equations in two unknowns, $u(x,y,t),\ v(x,y,t)$. In a bounded domain $\Omega \subset R^2$, with homogeneous boundary conditions on $\partial\Omega$, and no forcing term, this paper considers the following data assimilation/inverse design problem associated with that system: Find initial values $[u(.,0),\ v(.,0)]$ that can evolve into a close approximation to a desired target result $[u^*(.,T),\ v^*(.,T)]$, at an appropriately chosen $T > 0$. Here, highly non smooth target data are considered that *may not correspond to actual solutions* at time T, and it may not be possible to find such initial values. Such a 2D viscous Burgers problem has not previously been studied. For the 1D Burgers equation, data assimilation is discussed in [2–8], using various iterative methods. The significance of data assimilation in the geosciences is emphasized in [9].

*Applied and Computational Mathematics Division, National Institute of Standards and Technology, Gaithersburg, MD 20899. (alfred.carasso@nist.gov).

Following [1], for flows with kinematic viscosity ν, in bounded domains $\Omega \subset R^2$ with area A, over a time interval $[0,T]$, we define the Reynolds number RE as follows

$$\begin{aligned} &U_{max} = \max_{\Omega\times[0,T]} \left\{u^2(x,y,t) + v^2(x,y,t)\right\}^{1/2}, \\ &RE = U_{max}\sqrt{A}/\nu. \end{aligned} \tag{1}$$

Using a direct non-iterative method based on marching backward in time with a stabilized explicit finite-difference scheme [10–12], a large class of examples is presented where, with realistic values of $T > 0$, and Reynolds numbers as high as 18000, useful initial values can be found that evolve into good approximations to the desired target data, with modestly small $\mathcal{L}^1$ relative errors. Importantly, there are also unsuccessful examples.

In dissipative evolution equations $w_t = Lw$, there is a fundamental difference between the present data assimilation/inverse design problem, which seeks initial values leading to an arbitrary desired result $w^*(.,T)$, and the more familiar ill-posed backward recovery problem. In the latter case, one starts with relatively smooth data $w^*(.,T)$ that are known to closely approximate an actual solution $w(.,T)$. Rigorous uncertainty estimates [13–19], generally require the spatial derivatives of w to be sufficiently small on $[0,T]$, in addition to T itself, in order to achieve useful reconstruction. For example, in the case of the 1D Burgers equation,

$$\begin{aligned} &w_t = \nu w_{xx} - ww_x, \qquad 0 < x < 1, \quad 0 < t \le T, \\ &w(0,t) = w(1,t) = 0, \end{aligned} \tag{2}$$

where $\nu > 0$ is the kinematic viscosity, let $D = [0,1]\times[0,T]$. With *known small* $\delta > 0$, let $w_1(x,t),\ w_2(x,t)$, be two smooth solutions satisfying

$$\begin{aligned} &\max_{(x,t)\in D}\ \{|w_i|, |w_{ix}|, |w_{it}|\} \le E, \quad i = 1,2, \\ &\parallel w_1(.,T) - w_2(.,T) \parallel_2 \ \le \delta. \end{aligned} \tag{3}$$

Then, as shown in [19, Eq. (2.7)], with

$$K > 2\exp\{E/\nu + (E^4T^2)/(64\nu^2)\}, \tag{4}$$

one has the following uncertainty estimate at $t = T/2$,

$$\parallel w_1(.,T/2) - w_2(.,T/2) \parallel_2 \le K\sqrt{E\delta}. \tag{5}$$

Clearly, for small $\nu > 0$, and with typical values of δ found in practice, both E and (E^4T^2/ν^2) would need to be sufficiently small for useful recovery. A

similarly restrictive exponential factor $K^\dagger$ occurs in the estimate found in [18, Eq. (2.9)].

The data assimilation problem considered here is markedly different. The target data $w^*(x,T)$ may not be smooth, and may not correspond to an actual solution of Eq. (2) at time $T > 0$. With small ν, large E, and a possibly *large unknown* $\delta > 0$, finding useful initial values $w(x,0)$ that can evolve into a close approximation to $w^*(x,T)$, may not be feasible in view of Eqs. (4, 5). The rigorous uncertainty estimates given in [13–19], necessarily contemplate worse case error amplification scenarios, and may be overly pessimistic in individual cases. However, there are also examples of failure that tend to validate such estimates.

2 Use of computational examples based on sharp image data

As in [10–12], numerical experiments will be presented involving 8 bit, 256×256 pixel gray-scale images. As illustrated in Figure 1, many images of easily recognizable objects are defined by non-smooth intensity data $f(x,y)$, that would be quite difficult to synthesize mathematically. These images are not of bounded variation. Rather, as shown in [20], with $0 < \alpha < 0.7$, and $|h| = (h_1^2 + h_2^2)^{1/2}$, they belong to the Lipschitz class $\Lambda(\alpha, 1, \infty)$, of functions $f(x,y)$ satisfing

$$\int_{R^2} |f(x+h_1, y+h_2) - f(x,y)| dxdy \leq Const.\ |h|^\alpha, \quad |h| \downarrow 0, \tag{6}$$

while images of bounded variation require $\alpha = 1$. Such non smooth images pose significant challenges in ill-posed reconstruction, and they constitute an invaluable tool for *exploring* the possibility of computing a wide variety of dissipative evolution equations backward in time.

The approach to be used is based on marching backward in time from the given target data at time T, using an $O(\Delta t)$ explicit finite difference scheme. As is well-known [21, p. 59], for ill-posed initial value problems, every consistent stepwise marching scheme, whether explicit or implicit, is necessarily *unconditionally unstable*. However, as shown in [10–12], it is possible to stabilize explicit marching schemes by applying an appropriate compensating smoothing operator at each time step to quench the instability. This renders the scheme unconditionally *stable*, but slightly inconsistent. In backward reconstructions from relatively smooth data known to closely approximate the exact solutions at time T, the cumulative error caused by such smoothing is sufficiently small to allow for useful results. Unexpectedly, such stabilized schemes may sometimes be useful in data assimilation with non smooth targets at time T, by using more aggressive smoothing at each time step.

Below, we review the error bounds obtained in the recently developed schemes in [10–12]. Using a simplified linear analysis in Sections 4 and 5 below, it is shown how data assimilation may be feasible in some cases, with a proper choice

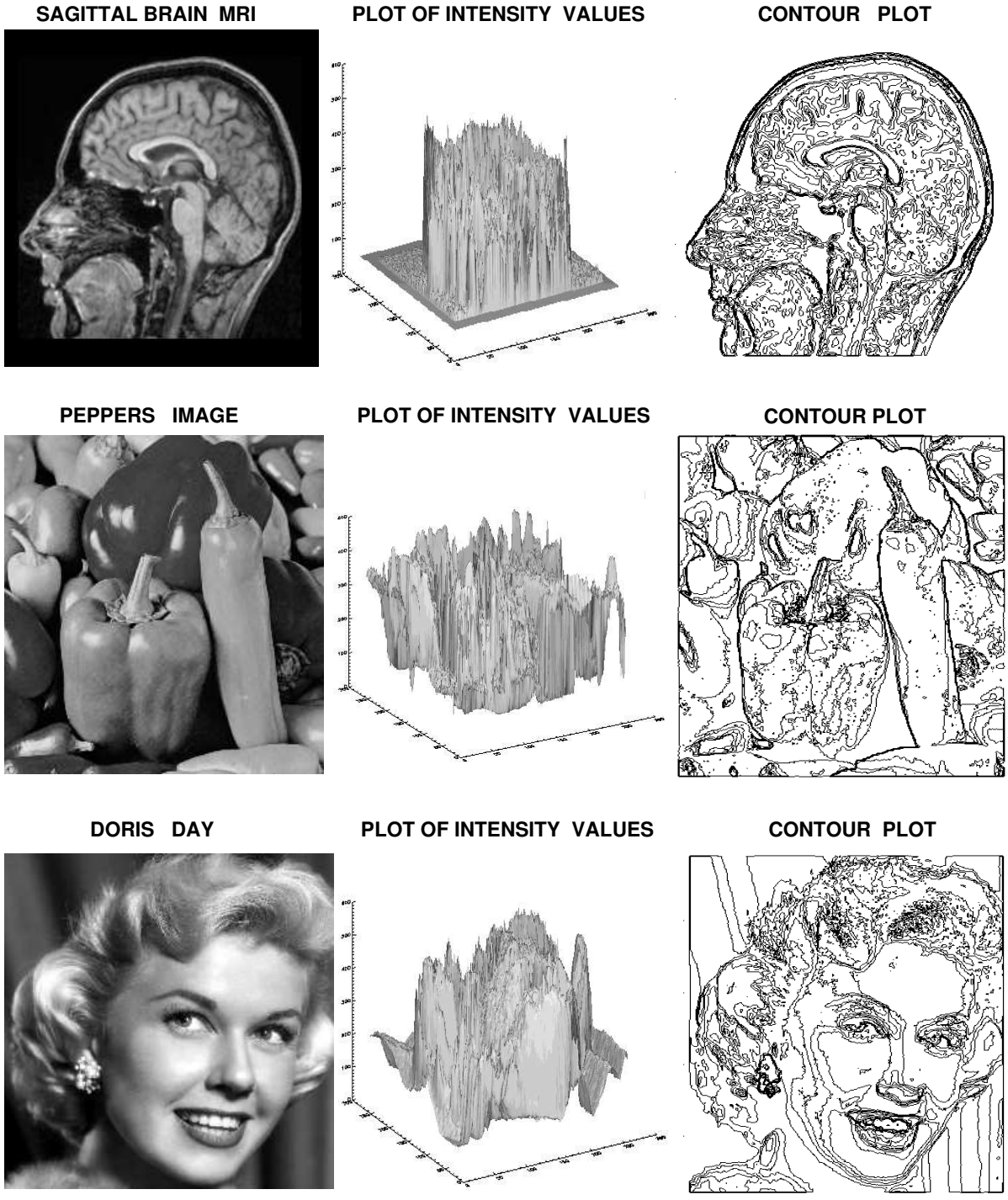

Figure 1: Many images of easily recognizable objects are defined by non-smooth intensity data, and are not of bounded variation, [20]. Such images pose significant computational challenges and provide instructive examples for exploring data assimilation.

of parameters in the smoothing operator. That simplified analysis is found helpful in Section 6, where nonlinear computational experiments are discussed.

3 Stepwise explicit schemes for 2D viscous Burgers' equation, marched forward or backward in time

Let Ω be the unit square in R^2 with boundary $\partial\Omega$. Let $< \ , \ >$ and $\| \ \|_2$, respectively denote the scalar product and norm on $\mathcal{L}^2(\Omega)$. With $\nu > 0$ the kinematic viscosity, consider the following 2D Burgers' system for $(x, y) \in \Omega$,

$$\begin{aligned} u_t &= L_1 u \equiv \nu\Delta u - uu_x - vu_y, \quad 0 < t \le T, \\ v_t &= L_2 v \equiv \nu\Delta v - uv_x - vv_y, \quad 0 < t \le T, \end{aligned} \tag{7}$$

together with homogeneous boundary conditions on $\partial\Omega$, and the initial values

$$u(x, y, 0) = u_0(x, y), \quad v(x, y, 0) = v_0(x, y), \quad (x, y) \in \Omega. \tag{8}$$

The well-posed forward initial value problem in Eq. (7) becomes ill-posed if the time direction is reversed. Such time-reversed computations are contemplated by allowing for possible *negative time steps* Δt in the explicit time-marching finite difference scheme described below. With N a positive integer, let $|\Delta t| = T/(N + 1)$ be the time step magnitude, and let $\tilde{u}^n(x, y) \equiv \tilde{u}(x, y, n\Delta t)$, $n = 0, 1, \cdots, N+1$, denote the intended approximation to $u(x, y, n\Delta t)$, and likewise for $\tilde{v}^n(x, y)$. It is helpful to consider Fourier series expansions for $\tilde{u}^n(x, y)$, $\tilde{v}^n(x, y)$, on the unit square Ω,

$$\tilde{u}^n(x, y) = \sum_{j,k=-\infty}^{\infty} \tilde{u}^n_{j,k} \exp\{2\pi i(jx + ky)\}, \tag{9}$$

with Fourier coefficients $\{\tilde{u}^n_{j,k}\}$ given by

$$\tilde{u}^n_{j,k} = \int_\Omega \tilde{u}^n(x, y) \exp\{-2\pi i(jx + ky)\} dxdy, \tag{10}$$

and similarly for $\tilde{v}^n(x, y)$. With given fixed $\omega > 0$ and $p > 1$, define $\lambda_{j,k}$, $\sigma_{j,k}$, as follows

$$\lambda_{j,k} = 4\pi^2\nu(j^2 + k^2), \qquad \sigma_{j,k} = \exp\{-2\omega|\Delta t|\lambda^p_{j,k}\}. \tag{11}$$

For any $f(x, y) \in \mathcal{L}^2(\Omega)$, let $\{f_{j,k}\}$ be its Fourier coefficients as in Eq (10). Using Eq. (11), define the linear operators P and S as follows

$$\begin{aligned} Pf &= \textstyle\sum_{j,k=-\infty}^{\infty} \lambda^p_{j,k} f_{j,k} \exp\{2\pi i(jx + ky)\}, \qquad \forall f \in \mathcal{L}^2(\Omega), \\ Sf &= \textstyle\sum_{j,k=-\infty}^{\infty} \sigma_{j,k} f_{j,k} \exp\{2\pi i(jx + ky)\}, \qquad \forall f \in \mathcal{L}^2(\Omega). \end{aligned} \tag{12}$$

The operator S is used as a stabilizing smoothing operator at each time step, in the following explicit time-marching finite difference scheme for the system in Eq (7), in which only the time variable is discretized, with possibly *negative time steps* Δt, while the space variables remain continuous,

$$\begin{aligned} \tilde{u}^{n+1} &= S\tilde{u}^n + \Delta t S L_1 \tilde{u}^n, \\ \tilde{v}^{n+1} &= S\tilde{v}^n + \Delta t S L_2 \tilde{v}^n, \qquad n = 0, 1, \cdots, N. \end{aligned} \tag{13}$$

The simplified linear analyses presented in Sections 4 and 5 below, are relevant to the above semi-discrete problem. In Section 6, where actual nonlinear computations are discussed, the space variables are also discretized, and FFT algorithms are used to synthesize the smoothing operator S.

4 Fourier stability analysis in linearized problem

Useful insight into the behavior of the nonlinear scheme in Eq. (13), can be gained by analyzing a related linear problem with constant coefficients. With positive constants $a,\ b$, consider the initial value problem on the unit square Ω,

$$\begin{aligned} u_t &= Lu \equiv \nu \Delta u - a u_x - b u_y, \quad 0 < t \le T, \\ u(x, y, 0) &= u_0(x, y), \end{aligned} \tag{14}$$

together with homogeneous boundary conditions on $\partial\Omega$. Let $|\Delta t| = T/(N+1)$. Unlike the case in Eq. (13), the stabilized marching scheme

$$\tilde{u}^{n+1} = S\tilde{u}^n + \Delta t S L \tilde{u}^n, \qquad n = 0, 1, \cdots, N, \tag{15}$$

with the *linear* operator L, and possibly *negative time steps* Δt, is susceptible to Fourier analysis. If $L\tilde{u}^n = f^n(x, y)$, then the Fourier coefficients $\{f^n_{j,k}\}$ satisfy $f^n_{j,k} = g_{j,k}\tilde{u}^n_{j,k}$, where, with $\lambda_{j,k}$ as in Eq. (11),

$$g_{j,k} = -\{\lambda_{j,k} + 2\pi i(aj + bk)\}. \tag{16}$$

Let R be the linear operator $R = S + \Delta t S L$. Then,

$$\begin{aligned} \tilde{u}^{n+1} &= R\tilde{u}^n \equiv \sum_{j,k=-\infty}^{\infty} \tilde{u}^n_{j,k}\{1 + \Delta t g_{j,k}\}\sigma_{j,k}, \\ \| \tilde{u}^{n+1} \|_2^2 &= \| R\tilde{u}^n \|_2^2 \le \sum_{j,k=-\infty}^{\infty} |\tilde{u}^n_{j,k}|^2 \{1 + |\Delta t||g_{j,k}|\}^2 \sigma^2_{j,k}, \end{aligned} \tag{17}$$

on using Parseval's formula.

In [10], detailed proofs are given for Lemma 1 and Theorems 1 and 2 stated below.

Lemma 1 *Let $\lambda_{j,k}$, $\sigma_{j,k}$, be as in Eq. (11), and let $g_{j,k}$ be as in Eq. (16). Choose a positive integer J such that if $\lambda_J = 4\pi^2\nu J$, we have*

$$max_{(j^2+k^2)\leq J}\ \{|g_{j,k}|\} \leq 2\lambda_J, \qquad |g_{j,k}| \leq 2\lambda_{j,k},\ \forall\ (j^2+k^2) > J. \tag{18}$$

With $p > 1$, choose $\omega \geq (\lambda_J)^{1-p}$ in Eq. (11). Then,

$$\sigma_{j,k}\,(1 + |\Delta t||g_{j,k}|) \leq 1 + 2|\Delta t|\lambda_J. \tag{19}$$

Hence, from Eq. (17), $\parallel R \parallel_2 \leq 1 + 2|\Delta t|\lambda_J$, and

$$\parallel \tilde{u}^n \parallel_2 = \parallel R^n u_0 \parallel_2 \leq \exp\{2n|\Delta t|\lambda_J\} \parallel u_0 \parallel_2, \qquad n = 1, 2, \cdots, N+1. \tag{20}$$

Therefore, with this choice of (ω, p), the explicit linear scheme in Eq. (15) is stable, marching forward or backward in time.

For functions $v(x, y, t)$ on $\Omega \times [0, T]$, define the norm $|||v|||_{2,\infty}$ as follows

$$|||v|||_{2,\infty} \equiv Sup_{0\leq t\leq T}\{\parallel v(\cdot, t) \parallel_2\}. \tag{21}$$

In Lemma 1, the finite difference approximation $\tilde{u}^n(x, y) \equiv \tilde{u}(x, y, n\Delta t)$ satisfies Eq. (15), whereas the exact solution $u^n(x, y) \equiv u(x, y, n\Delta t)$ in Eq. (14), satisfies $u^{n+1} = u^n + \Delta t L u^n + \tau^n$, where τ^n is the truncation error. We need to estimate the error $h^n(x, y) = u^n(x, y) - \tilde{u}^n(x, y),\ n = 0, 1, \cdots, N+1$.

Theorem 1 *With $\Delta t > 0$, let $u^n(x, y)$ be the unique solution of Eq. (14) at $t = n\Delta t$. Let $\tilde{u}^n(x, y)$ be the corresponding solution of the forward explicit scheme in Eq. (15), let p, λ_J, ω, be as in Lemma 1, and let P be as in Eq. (12). If $h^n(x, y) = u^n(x, y) - \tilde{u}^n(x, y)$, denotes the error at $t = n\Delta t$, $n = 1, 2, \cdots, N+1$, we have*

$$\begin{aligned} \parallel h^n \parallel_2 \leq\ & e^{2t\lambda_J} \parallel h^0 \parallel_2 + \left\{\omega(e^{2t\lambda_J} - 1)/\lambda_J\right\} |||Pu|||_{2,\infty} \\ +\ & \left\{(e^{2t\lambda_J} - 1)/2\lambda_J\right\} \left\{2\omega\Delta t\ |||PLu|||_{2,\infty} + (\Delta t/2)\ |||L^2 u|||_{2,\infty}\right\}. \end{aligned} \tag{22}$$

Define the constants $K1,\ K2,\ K3,\ K4,\ K5$, as follows

$$K1 = e^{2T\lambda_J},\quad K2 = \{\omega(e^{2T\lambda_J} - 1)/\lambda_J\},\quad K3 = |\Delta t|K2,\quad K4 = K3/(4\omega),$$

$$K5 = K2\ |||Pu|||_{2,\infty} + K3\ |||PLu|||_{2,\infty} + K4\ |||L^2 u|||_{2,\infty}. \tag{23}$$

It follows from Eq. (22) in Theorem 1 that in the forward problem, the error $h^{N+1}(x, y)$ at time $T = (N+1)\Delta t$ satisfies

$$\parallel h^{N+1} \parallel_2 \leq K1 \parallel h^0 \parallel_2 + K5 \tag{24}$$

In Eq. (24), the error $h^0(x,y) \neq 0$, if the initial values $\tilde{u}^0(x,y)$ used in Eq. (15) differ from $u_0(x,y)$ in Eq. (14). In Eq. (23), the term $K2\ |||Pu|||_{2,\infty}$ is the *stabilization penalty*, and the constants $K3$ and $K4$ vanish as $|\Delta t| \downarrow 0$. The entries in Table 1 below will be found useful in the sequel.

TABLE 1

Values of constants $K1$ through $K4$ in Eq. (23), with following parameter choices:
$T = 2.0 \times 10^{-4},\ |\Delta t| = 1.25 \times 10^{-8},\ p = 3.25,\ \omega = 7.0 \times 10^{-9},\ \lambda_J = (\omega)^{1/(1-p)}.$

$K1 = e^{2T\lambda_J}$	$K2 = \{\omega(e^{2T\lambda_J} - 1)/\lambda_J\}$	$K3 = \lvert\Delta t\rvert K2$	$K4 = K3/(4\omega)$
$K1 < 5.4$	$K2 < 7.3 \times 10^{-12}$	$K3 < 9.2 \times 10^{-20}$	$K4 < 3.3 \times 10^{-12}$

In the ill-posed problem of marching backward from $t = T$ discussed in Theorem 2, it is assumed that the given data $\tilde{u}^0(x,y)$ at $t = T$, differ from the unknown exact data by an error $\gamma(x,y)$:

$$\tilde{u}^0(x,y) = u(x,y,T) + \gamma(x,y), \qquad \| \gamma \|_2 \leq \delta. \tag{25}$$

Theorem 2 *With $\Delta t < 0$, let $u^n(x,y)$ be the unique solution of the forward well-posed problem in Eq. (14) at $s = T - n|\Delta t|$. Let $\tilde{u}^n(x,y)$ be the corresponding solution of the backward explicit scheme in Eq. (15), with initial data $\tilde{u}^0(x,y) = u(x,y,T) + \gamma(x,y)$ as in Eq. (25). Let $p,\ \lambda_J,\ \omega$, be as in Lemma 1, and let P be as in Eq. (12). If $h^n(x,y) \equiv u^n(x,y) - \tilde{u}^n(x,y)$, denotes the error at $s = T - n|\Delta t|,\ \ n = 0, 1, 2, \cdots, N+1$, we have, with δ as in Eq.(25),*

$$\begin{aligned} \| h^n \|_2 \leq\ & \delta e^{2n|\Delta t|\lambda_J} + \left\{\omega(e^{2n|\Delta t|\lambda_J} - 1)/\lambda_J\right\} |||Pu|||_{2,\infty} \\ +\ & \left\{(e^{2n|\Delta t|\lambda_J} - 1)/2\lambda_J\right\} \{2\omega|\Delta t||||PLu|||_{2,\infty} + (|\Delta t|/2)|||L^2 u|||_{2,\infty}\} \end{aligned} \tag{26}$$

With the definitions given in Eq. (23), it follows from Eq. (26) that $h^{N+1}(x,y)$, the error at time $t = 0$ in the backward problem in Theorem 2, satisfies

$$\| h^{N+1} \|_2 \leq \delta K1 + K5 \tag{27}$$

5 Application to Data Assimilation

The methods in [10–12] together with Theorem 2 above, are aimed at backward in time reconstruction from data that are known to closely approximate the exact solution at time $T > 0$, and presuppose a *known small* $\delta > 0$ in Eq. (25). However, it may be possible to obtain useful results in the inverse design case

where $\tilde{u}^0(x,y)$ is the target data $u^*(x,y,T)$ in Eq. (25), and differs from some *unknown* exact data $u(x,y,T)$, by an unknown amount $\delta > 0$ that may be larger than expected. If such an unknown exact solution $u(x,y,t)$ does not have exceedingly large values for $|||Pu|||_{2,\infty}$, $|||PLu|||_{2,\infty}$, and $|||L^2u|||_{2,\infty}$, useful data assimilation may be feasible with proper choice of parameters in the smoothing operator S in Eq. (15). For example, with the parameter choices made in Table 1 above, the resulting values for the constants $K1$ through $K4$ may lead to a useful reconstruction $\tilde{u}(x,y,0)$ at time $t = 0$, differing from the exact value $u_0(x,y)$ in Eq. (14), by an $\mathcal{L}^2$ error $\delta K1 + K5$, according to Eq. (27). From Eqs. (23), and Table 1, the constant $K5$ may be negligible when compared to $\delta K1$.

Next, using the backward reconstruction $\tilde{u}(x,y,0)$ as initial data in the forward problem in Theorem 1, and using the above choice of parameters, leads to an approximation $\tilde{u}(x,y,T)$ at time T, differing from the unknown exact value $u(x,y,T)$ by an $\mathcal{L}^2$ error $[K1\ (\delta K1 + K5) + K5]$, according to Eq. (24). Hence,

$$\begin{aligned} \| \tilde{u}(.,T) - u^*(.,T) \|_2 &\leq \| \tilde{u}(.,T) - u(.,T) \|_2 + \| u(.,T) - u^*(.,T) \|_2 \\ &\leq \delta(1 + K1^2) + K5(1 + K1). \end{aligned} \tag{28}$$

Thus, if $K5$ is negligible, Theorem 2 produces initial data $\tilde{u}(x,y,0)$ that evolve into $\tilde{u}(x,y,T)$, approximating the given target data with an $\mathcal{L}^2$ error $\delta(1 + K1^2)$.

Remark. When data assimilation is feasible, the values of T, $|\Delta t|$, ω, p, and $\lambda_J = \omega^{1/(1-p)}$, play a decisive role. With the choices made in Table 1 above, one finds $(1 + K1^2) \approx 30.0$. However, with a smaller value of ω, such as $\omega = 3.0 \times 10^{-10}$, one would find $(1 + K1^2) \approx 86000$, and less successful data assimilation. Choosing a larger value of T, such as $T = 1.0 \times 10^{-3}$, would lead to $(1 + K1^2) \approx 2.0 \times 10^7$, and unsuccessful data assimilation.

6 2D nonlinear computational experiments

It remains to be seen whether the above simplified linear analysis is predictive of behavior in the coupled nonlinear system in Eq. (7). The three experiments discussed below involve use of the stabilized difference scheme in Eq. (13). An equispaced grid is placed on the unit square Ω, and second order accurate centered finite differencing is used for the space variables in the fully discrete nonlinear scheme. Fast Fourier Transform (FFT) algorithms are used to synthesize the smoothing operator S defined in Eq. (12). In each of the three experiments, the kinematic viscosity $\nu = 0.02$, and the target data are prescribed at time $T = 2.0 \times 10^{-4}$. All three experiments *fail* if the same data are prescribed at $T \geq 1.0 \times 10^{-3}$. In the 1D nonlinear Burgers equation, a restriction on T is implied in the stability estimate in Eqs. (4, 5).

All three experiments involve 256×256 pixel gray scale images, defined by non-smooth underlying intensity data, with integer values ranging between

zero and 255. These images have zero intensities on and near the boundary. With $\nu = 0.02$ and $A = 1$ in Eq. (1), this leads to a Reynolds Number $RE \approx 18000$. The 2D Burgers equation involves the evolution of two distinct images that interact with each other, which may produce unexpected results. With $|\Delta t| = 1.25 \times 10^{-8}$, we choose $p = 3.25,\ \omega = 7.0 \times 10^{-9}$, in the smoothing operator S in the nonlinear difference scheme in Eq. (13). This choice of parameters leads to the favorable values for $K1$ through $K4$, shown in Table 1 in the simplified linear analysis in Section 5. In these experiments, after every time step, the computed values are constrained to lie between zero and 255, by redefining all negative values to be zero, and all values exceeding 255 to be 255.

Sydney Opera House and Joan Crawford. This is illustrated in Figures 2 and 3, and documented in Table 2. The Sydney and Joan Crawford target data at time T are shown in the leftmost columns of these two Figures, as images and associated contour plots. Marching backward in time from these data, using Eq. (13), produced the curious results shown in the middle columns of Figures 2 and 3. Here, the distorted roof tops in the Sydney image, together with the new facial expression in the Joan Crawford image, were unanticipated. Such candidate initial values did not seem likely to evolve into the desired target data in the leftmost columns. Marching forward in time from these middle column data, using Eq. (13), resulted in the images and contour plots shown in the rightmost columns of Figures 2 and 3. Clearly, since the leftmost column data *do not* correspond to an actual solution of the 2D Burgers equation at time T, one cannot expect the rightmost column data to provide a close match. However, the Sydney rooftops and Joan Crawford's original facial expression, appear to have recovered.

Indeed, Table 2 provides important quantitative information. While the analysis given in Sections [3-5] involved the $\mathcal{L}^2$ norm, the present data assimilation approach is found to be better behaved in the $\mathcal{L}^1$ norm. The $\mathcal{L}^1(\Omega)$ norms of the images in the rightmost column closely approximate the correponding norms in the leftmost column. The $\mathcal{L}^1(\Omega)$ relative errors are 7.93% for the Sydney image and 8.49% for the Joan Crawford image, while the $\mathcal{L}^2(\Omega)$ relative errors are noticeably higher. Taken together, the rightmost images, contour plots, and $\mathcal{L}^1(\Omega)$ relative errors, indicate successful data assimilation in this example.

Mr Spock and Brain MRI. This is illustrated in Figures 4 and 5, and documented in Table 3. The Spock and Brain MRI target data at time T are shown in the leftmost columns of these two Figures, as images and associated contour plots. Marching backward in time from these data, using Eq. (13), produced the results shown in the middle columns of Figures 4 and 5. Here, the candidate Brain MRI image at $t = 0$, appears unexpectedly distorted. However, marching forward in time from these middle column data, using Eq. (13), resulted in the images and contour plots shown in the rightmost columns of Figures 4 and 5. The Mr Spock image in the rightmost column is surprisingly good, while much of the distortion in the Brain image seems to have been eliminated.

The quantitative information in Table 3 again confirms successful data assimilation in this example. The $\mathcal{L}^1(\Omega)$ norms of the desired target data have been closely approximated by the corresponding norms in the rightmost data, while the $\mathcal{L}^1(\Omega)$ relative errors are 6.96% for the Spock image and 9.15% for the Brain image. The $\mathcal{L}^2(\Omega)$ relative errors are again higher.

Alphanumeric image and USAF resolution chart. While numerous examples can be found of successful data assimilation with $\mathcal{L}^1(\Omega)$ relative errors $< 10\%$, there are also less succesful examples with $\mathcal{L}^1(\Omega)$ relative errors on the order of 20%. A highly *unsuccessful* example is illustrated in Figures 6 and 7, and documented in Table 4. The Alphanumeric and USAF chart target data at time T are shown in the leftmost columns of these two Figures, as images and associated contour plots. Marching backward in time from these data, using Eq. (13), produced the results shown in the middle columns of Figures 6 and 7. Here, while both candidate initial values are severely distorted, the Alphanumeric data are unintelligible, either as an image or a contour plot. Marching forward in time from these middle column data, using Eq. (13), resulted in the images and contour plots shown in the rightmost columns of Figures 6 and 7. The Alphanumeric data in the rightmost column remain largely indecipherable, and not a useful approximation to the target data.

In Table 4, we now find that the $\mathcal{L}^1(\Omega)$ norms in the rightmost data poorly approximate the corresponding norms in the target data, while the $\mathcal{L}^1(\Omega)$ relative errors are near 174% for the Alphanumeric image, and near 54% for the USAF chart image. The $\mathcal{L}^2(\Omega)$ relative errors are smaller, but nevertheless quite large. Repeating the above experiment with larger or smaller values of ω, did not noticeably change the outcome.

The evident failure in the above example appears to vindicate the rigorous uncertainty estimates developed in [13–19], and highlighted in Eqs. (4, 5) above.

7 Concluding remarks

With proper parameter choices, stabilized explicit schemes appear to be helpful in difficult data assimilation problems, involving non differentiable data, and such quasilinear parabolic equations as the 2D Burgers system. Future work should explore the possible application of explicit schemes to data assimilation/inverse design in other nonlinear parabolic problems of geophysical interest. Examples of failure in such data assimilation are also instructive and valuable.

Figure 2: Data assimilation of Sydney Opera House and Joan Crawford images. Desired data at time T, shown in leftmost column, is marched backward in time to obtain the candidate initial values shown in middle column. When marched forward in time, middle column data produces solution of 2D viscous Burgers equation at time T, shown in rightmost column. Quantitative error estimates for this experiment are provided in Table 2.

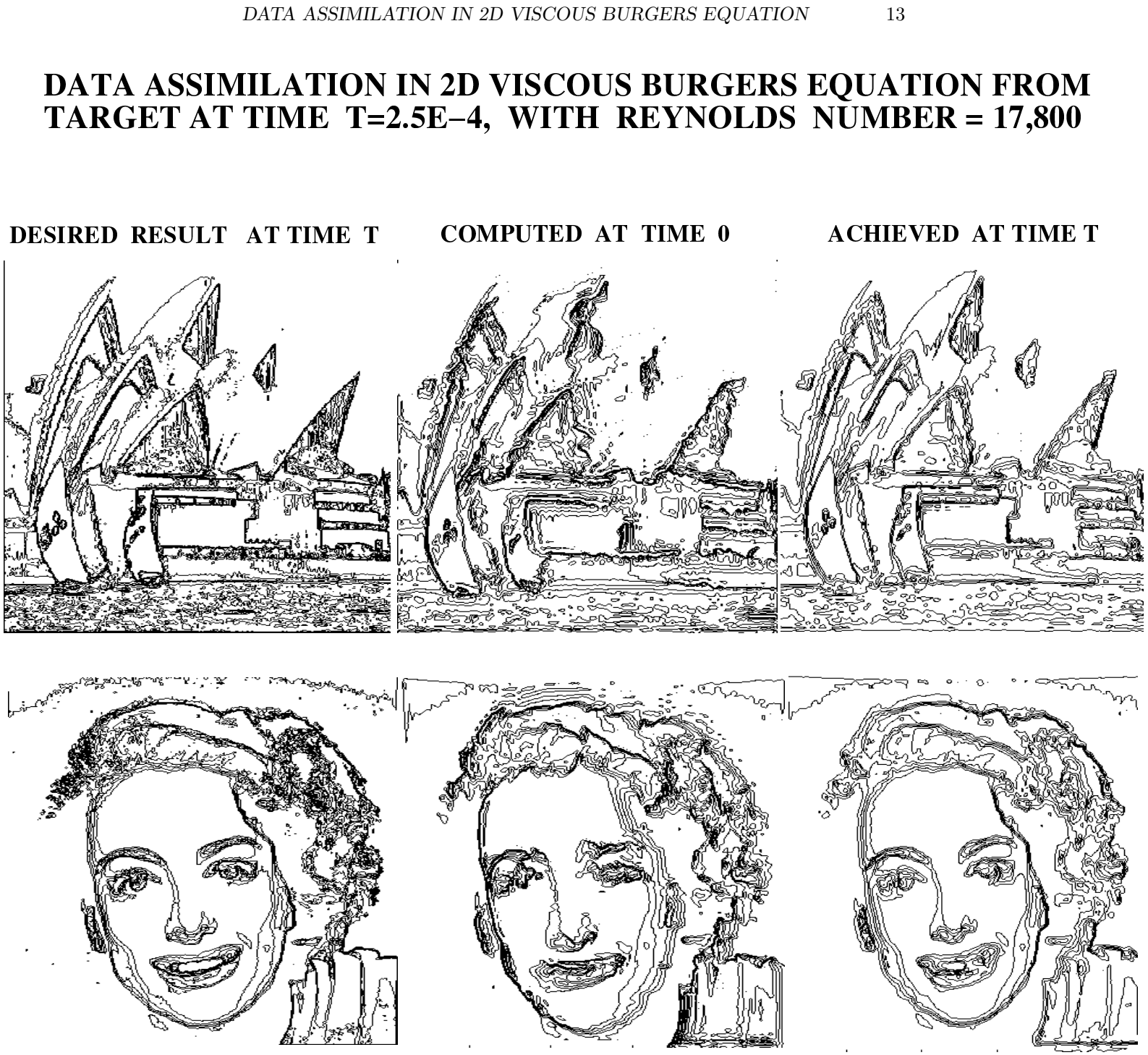

Figure 3: Associated contour plots in data assimilation experiment described in Figure 2.

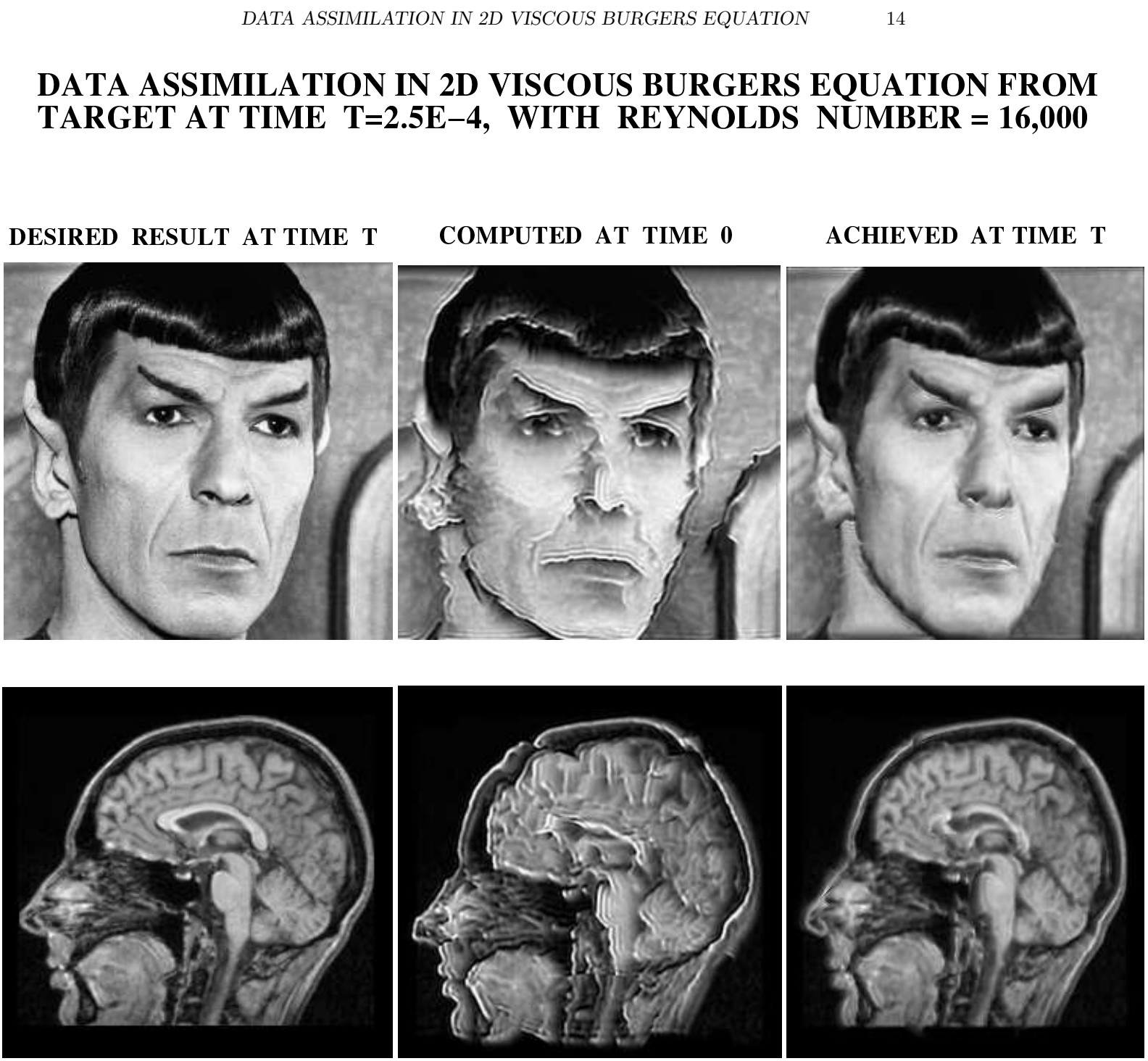

Figure 4: Data assimilation of Mr Spock and Brain MRI images. Desired data at time T, shown in leftmost column, is marched backward in time to obtain the candidate initial values shown in middle column. When marched forward in time, middle column data produces solution of 2D viscous Burgers equation at time T, shown in rightmost column. Quantitative error estimates for this experiment are provided in Table 3.

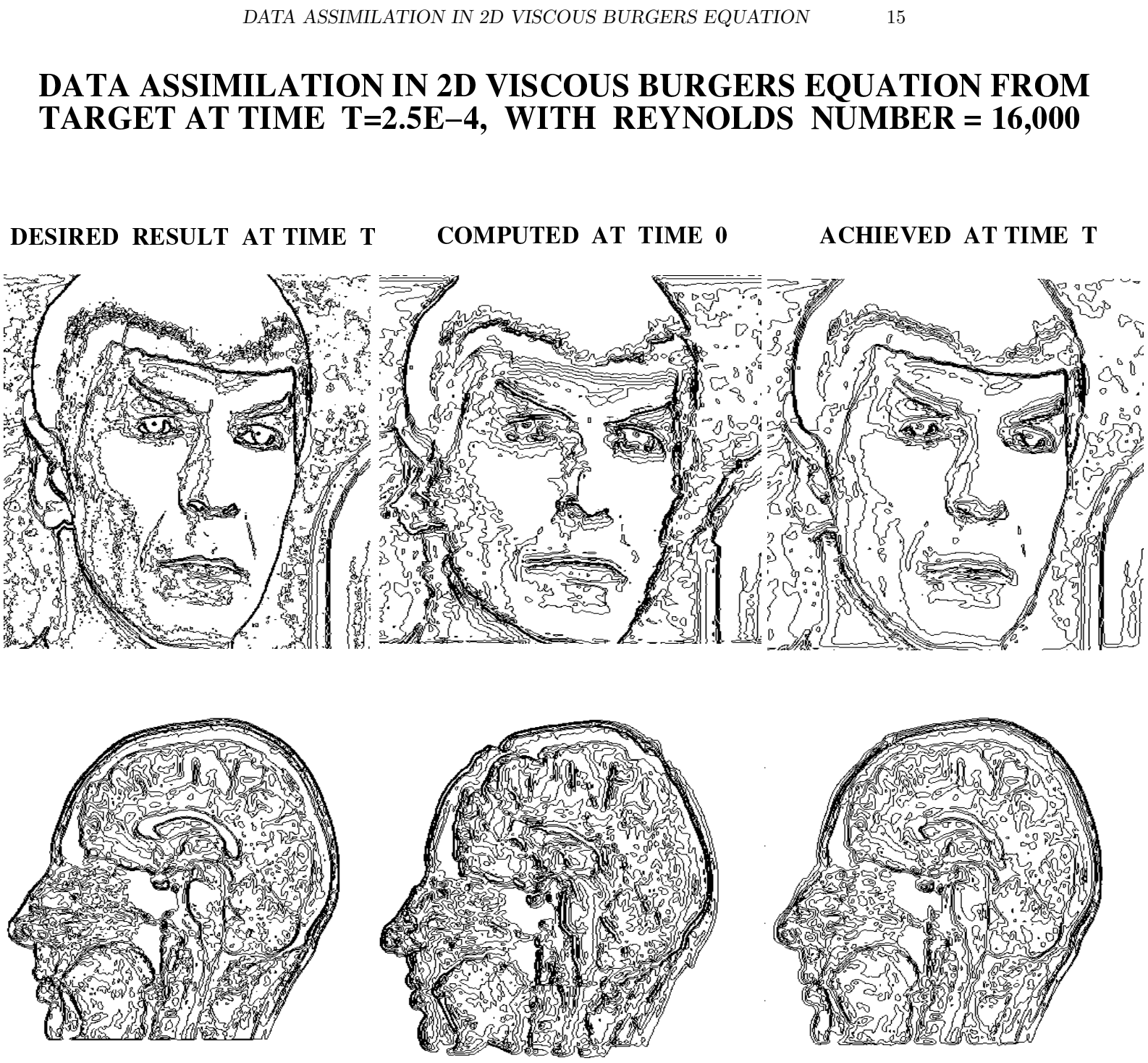

Figure 5: Associated contour plots in data assimilation experiment described in Figure 4.

FAILURE IN DATA ASSIMILATION IN 2D BURGERS EQUATION FROM TARGET AT TIME T=2.5E−4, WITH REYNOLDS NUMBER = 18,000

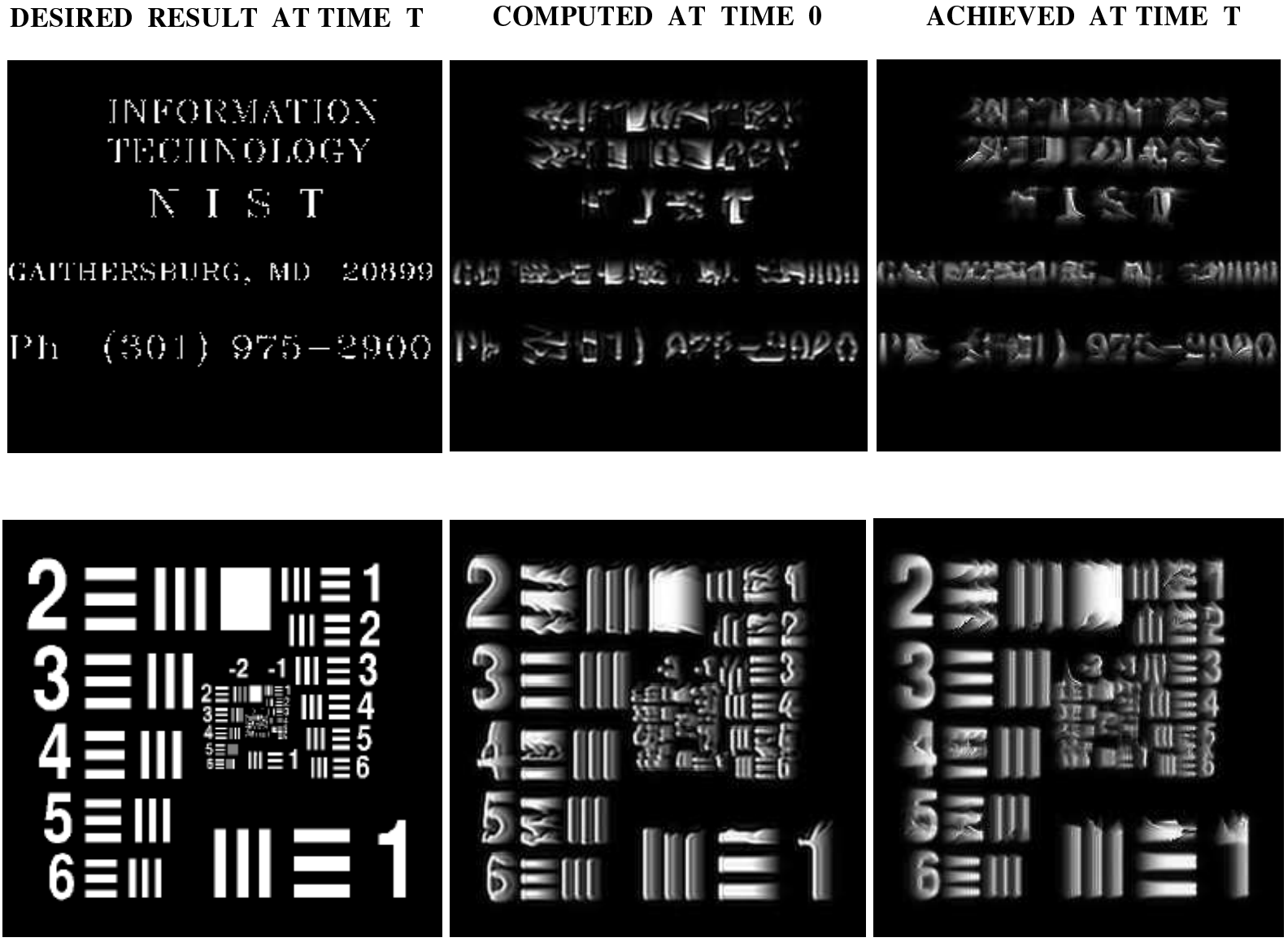

Figure 6: Data assimilation of Alphanumeric and USAF Chart images. Desired data at time T, shown in leftmost column, is marched backward in time to obtain the candidate initial values shown in middle column. When marched forward in time, middle column data produces solution of 2D viscous Burgers equation at time T, shown in rightmost column. Quantitative error estimates for this experiment are provided in Table 4.

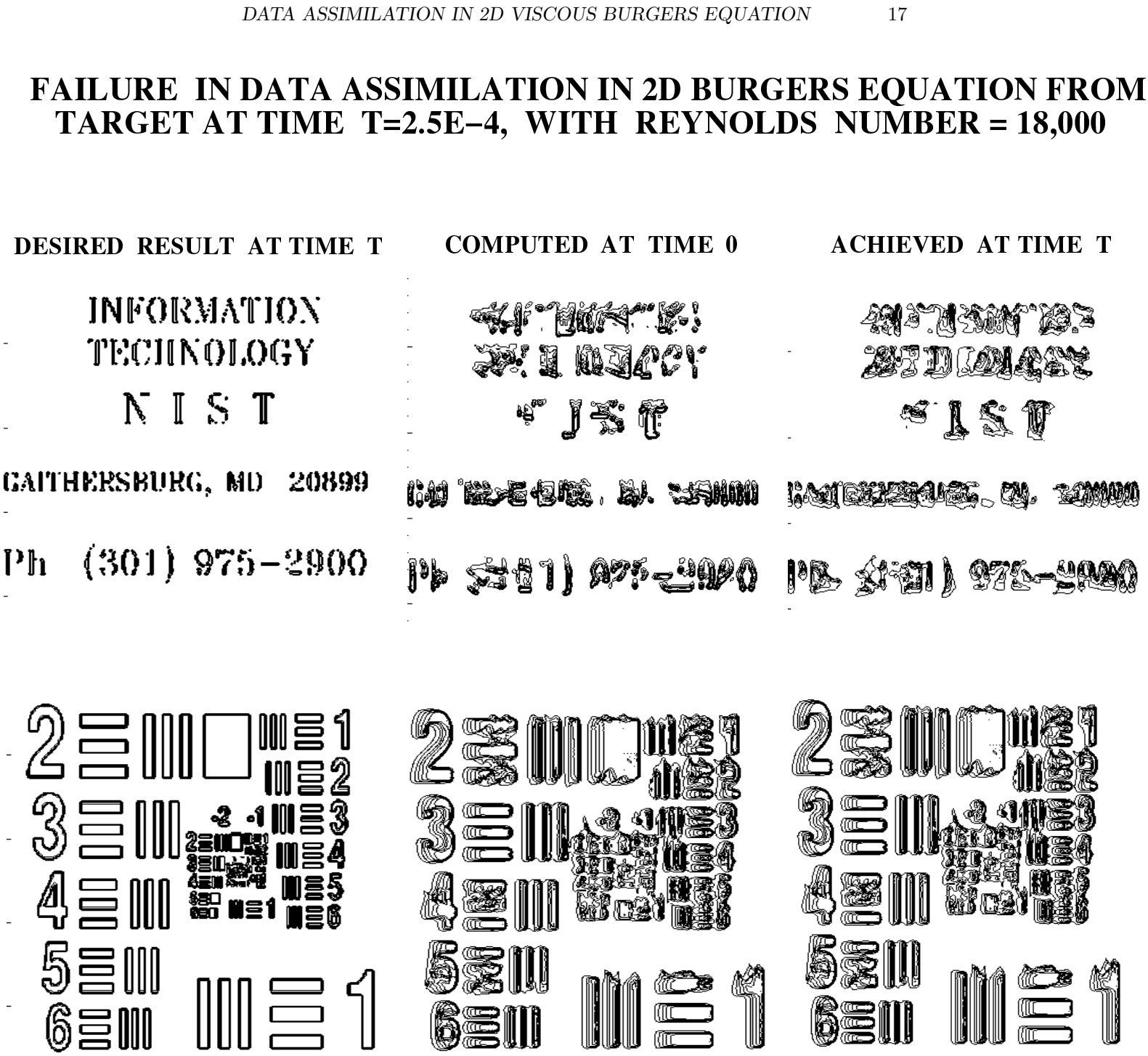

Figure 7: Associated contour plots in data assimilation experiment described in Figure 6.

TABLE 2
Sydney Opera House and Joan Crawford at RE=17800.
$\mathcal{L}^1$-norm behavior in data assimilation from non smooth target at $T = 2.0 \times 10^{-4}$.

Image	*Target $\mathcal{L}^1$ norm*	*Achieved $\mathcal{L}^1$ norm*	*$\mathcal{L}^1$ Rel Err*	*$\mathcal{L}^2$ Rel Err*
Sydney	156.33	155.16	7.93%	12.05%
Crawford	80.26	80.46	8.49%	11.74%

TABLE 3
Mr Spock and Brain MRI at RE=16000.
$\mathcal{L}^1$-norm behavior in data assimilation from non smooth target at $T = 2.0 \times 10^{-4}$.

Image	*Target $\mathcal{L}^1$ norm*	*Achieved $\mathcal{L}^1$ norm*	*$\mathcal{L}^1$ Rel Err*	*$\mathcal{L}^2$ Rel Err*
Spock	123.78	123.42	6.96%	10.54%
Brain MRI	58.97	59.31	9.15%	11.68%

TABLE 4
Alphanumeric and USAF Chart at RE=18000.
$\mathcal{L}^1$-norm behavior in data assimilation from non smooth target at $T = 2.0 \times 10^{-4}$.

Image	*Target $\mathcal{L}^1$ norm*	*Achieved $\mathcal{L}^1$ norm*	*$\mathcal{L}^1$ Rel Err*	*$\mathcal{L}^2$ Rel Err*
Alphanum	8.16	13.06	173.55%	83.42%
USAF	46.73	43.35	53.76%	43.34%

References

[1] Cole JD. On a quasi-linear parabolic equation occurring in aerodynamics. Quart. Appl. Math. 1951;3:225–236.

[2] Lundvall J, Kozlov V, Weinerfelt P. Iterative methods for data assimilation for Burgers' equation. J. Inverse Ill-Posed Probl. 2006;14:505–535.

[3] Auroux D, Blum J. A nudging-based data assimilation method for oceanographuc problems: the back and forth nudging (BFN) algorithm. Proc. Geophys. 2008;15:305–319.

[4] Ou K, Jameson A. Unsteady adjoint method for the optimal control of advection and Burgers' equation using high order spectral difference method. 49th AIAA Aerospace Science Meeting, 4-7 January 2011. Orlando, Florida.

[5] Auroux D, Nodet M. The back and forth nudging algorithm for data assimilation problems: theoretical results on transport equations. ESAIM:COCV 2012;18:318–342.

[6] Auroux D, Bansart P, Blum J. An evolution of the back and forth nudging for geophysical data assimilation: application to Burgers equation and comparison. Inverse Probl. Sci. Eng. 2013;21:399-419

[7] Allahverdi N, Pozo A, Zuazua E. Numerical aspects of large-time optimal control of Burgers' equation. ESAIM Mathematical Modeling and Numerical Analysis 2016;50:1371–1401.

[8] Gosse L, Zuazua E. Filtered gradient algorithms for inverse design problems of one-dimensional Burgers' equation. Innovative Algorithms and Analysis 2017;197–227.

[9] de Campos Velho HF, Barbosa VCF, Cocke S. Special issue on inverse problems in geosciences. Inverse Probl. Sci. Eng. 2013;21:355-356. DOI:10.1080/17415977.2012.712532

[10] Carasso AS. Stable explicit stepwise marching scheme in ill- posed time-reversed 2D Burgers' equation. Inverse Probl. Sci. Eng. 2019;27:1672-1688

[11] Carasso AS. Computing ill-posed time-reversed 2D Navier-Stokes equations, using a stabilized explicit finite difference scheme marching backward in time. Inverse Probl. Sci. Eng. 2019; DOI:10.1080/17415977.2019.1698564

[12] Carasso AS. Stabilized leapfrog scheme run backward in time, and the explicit $O(\Delta t)^2$ stepwise computation of ill-posed time-reversed 2D Navier-Stokes equations. Inverse Probl. Sci. Eng. 2021; DOI:10.1080/17415977.2021.1972997

[13] Ames KA, Straughan B. Non-Standard and Improperly Posed Problems. New York (NY): Academic Press; 1997.

[14] Knops RJ, Payne LE. On the stability of solutions of the Navier-Stokes equations backward in time. Arch. Rat. Mech. Anal. 1968;29:331–335.

[15] Payne LE. Uniqueness and continuous dependence criteria for the Navier-Stokes equations. Rocky Mountain J. Math. 1971;2:641–660.

[16] Payne LE. Some remarks on ill-posed problems for viscous fluids. Int. J. Engng Sci. 1992;30:1341–1347.

[17] Carasso AS. Reconstructing the past from imprecise knowledge of the present: Effective non-uniqueness in solving parabolic equations backward in time. Math. Methods Appl. Sci. 2012;36:249-261.

[18] Carasso A. Computing small solutions of Burgers' equation backwards in time. J. Math. Anal. App. 1977;59:169–209.

[19] Hào DN, Nguyen VD, Nguyen VT. Stability estimates for Burgers-type equations backward in time. J. Inverse Ill Posed Probl. 2015;23:41–49.

[20] Carasso AS, Vladár AE. Calibrating image roughness by estimating Lipschitz exponents, with applications to image restoration. Opt Eng 2008;47:037012.

[21] Richtmyer RD, Morton KW. Difference Methods for Initial Value Problems. 2nd ed. New York (NY): Wiley; 1967.